Electromagnetic effects on plasma microturbulence and transport

P. B. Snyder[a)]
General Atomics, P.O. Box 85608, San Diego, California 92186

G. W. Hammett
Princeton Plasma Physics Laboratory, Princeton University, P.O. Box 451, Princeton, New Jersey 08543

(Received 25 September 2000; accepted 27 November 2000)

Results are presented from three-dimensional kinetic-fluid simulations of pressure gradient driven microturbulence in toroidal long mean-free-path plasmas. A numerically efficient model which includes self-consistent magnetic fluctuations and nonadiabatic electron dynamics is employed. A transition from electrostatic ion-drift turbulence to Alfvénic turbulence is seen at modest values of the plasma pressure. Significant electromagnetic effects on heat conductivity are observed, including an increase as the ideal ballooning threshold is approached, particularly when electron Landau damping is included. Turbulent spectra show a number of similarities to experimental fluctuation measurements. © *2001 American Institute of Physics.* [DOI: 10.1063/1.1342029]

I. INTRODUCTION

A quantitative physical understanding of turbulent transport in magnetized plasmas is crucial to the analysis of present experiments and the design of future fusion devices. Therefore, substantial effort has been invested in the development of increasingly realistic numerical simulations of plasma turbulence in the hot interior of fusion relevant plasmas.[1–7] These simulations employ analytic techniques which reduce the dimensionality of the phase space, and which remove many of the widely disparate spatial and temporal physical scales characteristic of magnetized, collisionless plasma.[8–12] Past simulations have led to rapidly expanding understanding of plasma turbulence and transport, though limitations remain. In past three-dimensional (3D) ion temperature gradient (ITG) microturbulence simulations for the core (in the long mean-free-path regime), fluctuations have often been assumed to be purely electrostatic. However, magnetic fluctuations are well known to both alter the dynamics of primarily electrostatic instabilities such as the ITG mode,[13–17] and introduce electromagnetic instabilities such as the kinetic ballooning mode (KBM),[18–23] the kinetic analog of the ideal ballooning mode. Furthermore, the electrostatic approximation requires not only that the ratio of plasma to magnetic pressure (β) be small, but also that β be far below the ideal magnetohydrodynamic (MHD) critical β_c for linear instability.[17] Hence this approximation can be expected to break down both in the interior of a high β plasma, and in any region where pressure gradients are sharp enough to push the plasma close to ideal instability, as often occurs in core transport barriers and in the edge region.

Interesting fluid simulations of the collisional outer edge region have demonstrated that self-consistent magnetic fluctuations are critical for prediction of edge transport (see Refs. 24–27 and references therein for a more complete discussion of recent work in this area). This, along with the likelihood that an attractive fusion device would have both high interior β and interior transport barriers, strongly motivates the development of a practical model for core turbulence including magnetic fluctuations. In the hot plasma core, the collisional fluid methods often used in the edge region are not strictly valid (though they have been useful for giving insight and guiding other research). Furthermore, the wide separation between the fast electron transit timescale and the slower ion drift and Alfvénic turbulence timescales makes direct simulation via kinetic, gyrokinetic, or gyrofluid methods challenging. Most previous core nonlinear 3D simulations with detailed ion dynamics (such as needed to get ITG modes and Landau damping accurately) have assumed electrostatic fields and adiabatic passing electrons in order to avoid explicitly treating electron dynamics along the field. Electromagnetic simulations must include passing electron dynamics along the field because electrons carry the dominant current perturbations which drive magnetic fluctuations. Here we develop a method which employs an expansion in the electron to ion mass ratio, allowing for practical simulations of core turbulence including self-consistent electromagnetic fluctuations and nonadiabatic passing electron dynamics.

II. PHYSICS MODEL

The electromagnetic electron Landau fluid and ion gyrofluid model employed is derived and described in detail in Refs. 28 and 29, and will only be briefly summarized here.

Electron equations are derived by taking velocity space moments of the drift kinetic equation. We wish to study turbulence on ion drift and shear Alfvén wave scales, and therefore impose the following ordering:

$$k_\perp^{-1} \sim \rho_i \sim \frac{c}{\omega_{pi}} \gg \rho_e, \quad \frac{c}{\omega_{pe}}, \tag{1}$$

where $k_\perp$ is a typical wave number perpendicular to the magnetic field, ρ is the gyroradius, ω_p is the plasma frequency, and the subscripts i and e refer to ions or electrons. The fluctuation frequency (ω) is ordered as follows:

a)Electronic mail: snyder@fusion.gat.com

$$\omega \sim k_\parallel v_{ti} \sim \omega_* \sim \omega_{Di,e} \sim k_\parallel c_s \sim k_\parallel v_A \ll k_\parallel v_{te} \sim \omega_{\mathrm{ETG}}, \quad (2)$$

where $v_t = \sqrt{T_0/m}$ is the thermal speed, ω_D is the combined curvature and ∇B drift frequency, c_s is the sound speed, $v_A = B/\sqrt{4\pi n_0 m_i}$ is the Alfvén speed, and the subscript 0 designates the equilibrium value. We define ω_{ETG} to be a frequency characteristic of the electron temperature gradient (ETG) mode. These short wavelength modes typically have $k_\theta \sim 1/\rho_e$, and hence $\omega_{\mathrm{ETG}} \sim \sqrt{m_i/m_e}\,\omega_*$, where ω_* is the diamagnetic frequency taken with $k_\theta \rho_i \sim 1$. The separation of scales between the Alfvén frequency and the electron transit frequency (and equivalently between ρ_i and the electron skin depth) requires $\beta_e \gg 2m_e/m_i$. This condition, along with $\omega_* \ll k_\parallel v_{te}$, is typically well satisfied in the core of a fusion relevant plasma, but may be violated in the outer edge region.

The above ordering is implemented by taking β to be $\mathcal{O}(1)$, and expanding in the electron to ion mass ratio. We neglect $\delta B_\parallel$ perturbations, which may be important for $\beta \gtrsim 10\%$, although a straightforward extension of the present model could be developed. Retaining the lowest order terms and those that are smaller by $\mathcal{O}(\sqrt{m_e/m_i})$, leads to the normalized electron continuity and momentum equations,

$$\frac{\partial n_e}{\partial t} + \mathbf{v}_E \cdot \nabla n + B \tilde{\nabla}_\parallel \frac{u_{\parallel e}}{B} - i\omega_* \phi + 2i\omega_d \left[\phi - \frac{n_e}{\tau} - T_e^{(0)} - \frac{T_{e\perp}^{(1)}}{2} - \frac{T_{e\parallel}^{(1)}}{2} \right] = 0, \quad (3)$$

$$\frac{\partial A_\parallel}{\partial t} + \tilde{\nabla}_\parallel \left[\phi - \frac{n_e}{\tau} - T_e^{(0)} - T_{e\parallel}^{(1)} \right] - (1+\eta_e) \frac{i\omega_* A_\parallel}{\tau} = \mathcal{C}_{ei}. \quad (4)$$

Here $\mathbf{v}_E$ is the $\mathbf{E} \times \mathbf{B}$ drift velocity, $\mathbf{B} = B\hat{\mathbf{b}}$ is the equilibrium magnetic field, $\tau = T_{i0}/T_{e0}$, and $\eta_{i,e}$ is the ratio of equilibrium density to temperature scale lengths ($\eta_{i,e} = L_n/L_{T_{i,e}}$). We define the gradient operator along the total magnetic field $\tilde{\nabla}_\parallel \doteq \hat{\mathbf{b}} \cdot \nabla - \hat{\mathbf{b}} \times \nabla A_\parallel \cdot \nabla$, the diamagnetic operator $i\omega_* \doteq -(\rho_i v_{ti}/n_0) \nabla n_0 \cdot \hat{\mathbf{b}} \times \nabla$, and the ∇B and curvature drift operator $i\omega_d \doteq (\rho_i v_{ti}/B^2)\, \mathbf{B} \times \nabla B \cdot \nabla$. The fluctuating electron density (n_e), parallel fluid velocity ($u_{\parallel e}$), temperature (T_e), electrostatic potential (ϕ), and parallel magnetic potential ($A_\parallel$) are normalized as follows:

$$(n_e, u_{\parallel e}, T_e, \phi, A_\parallel) = \frac{L_n}{\rho_i} \left(\frac{\tilde{n}_e}{n_0}, \frac{\tilde{u}_e}{v_{ti}}, \frac{\tilde{T}_e}{T_{0i}}, \frac{e\tilde{\phi}}{T_{0i}}, \frac{\tilde{A}_\parallel}{\rho_i B} \right), \quad (5)$$

where a tilde denotes the unnormalized fluctuating quantities. The operators are made dimensionless by normalization to the electron density scale length (L_n) and v_{ti}.

The lowest order fluctuating electron temperature $T_e^{(0)}$ is extracted via numerical inversion of the isothermal condition along the field line, $\tilde{\nabla}_\parallel [T_e^{(0)} + T_{0e}] = \tilde{\nabla}_\parallel T_e^{(0)} - \eta_e i\omega_* A_\parallel = 0$, which arises from the dominant terms in the higher moment equations. It is assumed that any fluctuating component of T_e which is constant on a field line does not contribute significantly to the $\omega_d T_e$ term in Eq. (3). The next order corrections to the temperature, $T_{e\parallel}^{(1)}$ and $T_{e\perp}^{(1)}$, can also be extracted from the full set of electron moment equations, closed with an appropriate toroidal Landau closure such as that in Ref. 3. In this work, only the parallel Landau damping correction in the momentum equation, $\tilde{\nabla}_\parallel T_{e\parallel}^{(1)} \to \sqrt{\pi/2}\sqrt{m_e/m_i}\,|k_\parallel| u_{\parallel e}$ is kept. The Landau damping term is written in Fourier space for conciseness; it becomes a convolution integral in real space. Neglecting this electron Landau damping term (formally taking $m_e/m_i \to 0$) leads to a model which is isothermal along the field. Numerical simulations are carried out both with and without this term. Electron-ion collisions are modeled by the simple operator $\mathcal{C}_{ei} = \hat{\nu}_{ei}(u_{\parallel e} - u_{\parallel i})$.

This electron model is both relatively simple and practical for implementation in numerical simulations, as it introduces neither the short timescales associated with electron free streaming along the field, nor the small spatial scales associated with the electron gyroradius and skin depth. Furthermore, the model represents a significant improvement over the adiabatic passing electron response used in most past simulations. In addition to finite-β effects and Alfvén wave dynamics, the model incorporates electron $\mathbf{E} \times \mathbf{B}$, curvature and ∇B drift motion, as well as linear electron Landau damping and the dominant $\mathbf{E} \times \mathbf{B}$ and magnetic flutter nonlinearities. The model is intended to describe only the untrapped electron distribution, and it treats the variation of $|B|$ along the field as a small perturbation ($\nabla_\parallel \ln B \sim \sqrt{m_e/m_i}$). Coupling to an appropriate trapped electron model is an important direction for future work.

It will be useful to benchmark results using this electron Landau closure with recently developed, fully kinetic electromagnetic turbulence simulations,[7] which may soon be run for the core plasma parameters we consider here. Improved versions of the electron Landau damping model (such as including an integral convolution representation to evaluate the $|k_\parallel|$ operator along perturbed field lines[30]) could eventually be tried. In the present form, the full electron model can be viewed as an extension of the work of Kadomtsev and Pogutse[31] to incorporate toroidal drifts, parallel ion flow, and an improved Landau damping model which phase mixes $\mathbf{E} \times \mathbf{B}$ driven perturbations.[12] This electron Landau damping model looks similar to an enhanced resistivity, with an enhancement factor of $|k_\parallel| v_{te}/\nu_{ei} \sim 10^2$ for typical core tokamak parameters. The range of resonant electron velocities $\Delta v_\parallel \sim \omega/k_\parallel \ll v_{te}$ is fairly small in the core, and one might worry about nonlinear particle trapping causing electron Landau damping to turn off. However, even a small amount of collisions can be important for such narrow resonances. The rate of scattering out of the resonant region is $\nu_{ei} v_e^2/(\Delta v_\parallel)^2$, and for a wide range of core parameters this is large compared to relevant linear or nonlinear rates even though ν_{ei} is small. While one would thus expect linear Landau damping to hold, nonlinear kinetic effects can be subtle, and comparisons between the results presented here and fully kinetic calculations including collisions will be interesting future work.

Ion dynamics are described by an electromagnetic gyrofluid model, though a direct gyrokinetic method could be substituted (an approach which is being explored by Chen and Parker[32]). The ion equations are derived by taking six moments of the electromagnetic gyrokinetic equation[9,11,33] and employing Landau closure models. Landau closures have

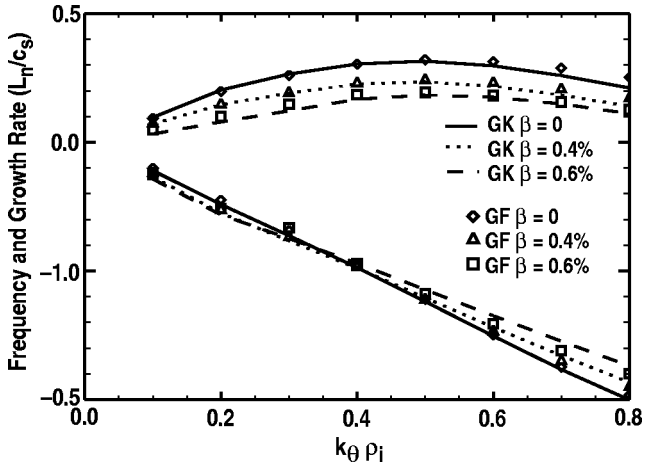

FIG. 1. Linear growth rate (positive) and frequency (negative) spectra of the toroidal ITG mode, for $\beta=0$, $\beta=0.4\%$, and $\beta=0.6\%$. The gyrofluid (GF) result is compared with results from the GS2 linear gyrokinetic code (GK).

been developed over time for various limits.[12,34,35,3,4] Here we use the Landau closures of Ref. 3, and are currently investigating recent neoclassical improvements[1] for the electromagnetic case. [The simulations reported here employ the large aspect ratio limit ($r/R\rightarrow 0$) in which neoclassical effects vanish.] The resulting ion equations, given in Refs. 28 and 29, are similar to Refs. 3 and 4, with the addition of magnetic induction terms and with $\nabla_\parallel \rightarrow \tilde{\nabla}_\parallel = \hat{\mathbf{b}}\cdot\nabla - \hat{\mathbf{b}}\times\nabla A_\parallel \cdot \nabla$ to include linear and nonlinear magnetic flutter effects. The gyrokinetic Poisson equation and Ampere's Law close the system.[8,10,11,33,36]

III. BENCHMARKS

The complete electron and ion ''gyrofluid'' model is benchmarked against linear gyrokinetic theory, as a check on both the accuracy of the gyrofluid physics model and its numerical implementation in toroidal geometry. Figure 1 shows a comparison of linear growth rate (γ) and frequency (ω) spectra of the ITG mode with the GS2 kinetic code,[37] using the parameters $\eta_i=\eta_e=5$, $R/L_n=3$, $s=1$, $q=2$, $m_e/m_i=0$, and $\tau=1$, where s is the magnetic shear and q is the safety factor. Trapped electrons, not included in the model, are neglected in the benchmark by setting the inverse aspect ratio (r/R) to zero. The comparison is undertaken at three values of $\beta=0\%,0.4\%,0.6\%$, with the gyrofluid model successfully reproducing the substantial finite-β stabilization of the ITG mode which occurs below the ideal MHD β limit (0.7% in this case).

The gyrofluid model also reproduces the correct linear behavior of the kinetic ballooning mode (KBM), an instability in the shear Alfvén branch of the dispersion relation driven by the pressure gradient and kinetic effects. Figure 2 shows comparisons with kinetic theory,[22] with $R/L_n=4$, $s=1$, $q=2$, $\tau=1$, and $k_\theta\rho_i=0.5$. Figure 2(a) shows a case with flat temperature profiles ($\eta_i=\eta_e=0$) where the KBM goes unstable precisely at the ideal MHD ballooning limit. In Fig. 2(b), a finite ion temperature gradient ($\eta_i=2$) drives the KBM unstable below the ideal ballooning limit due to an ion drift resonance effect.[38] This effect may drive significant

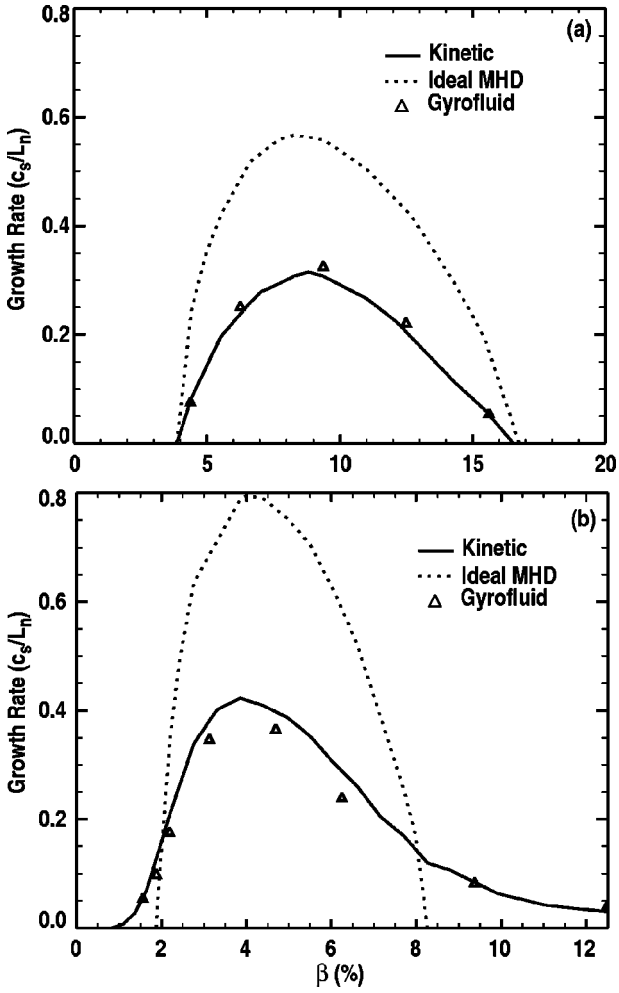

FIG. 2. Growth rate vs β for the KBM, with (a) $\eta_i=0$, (b) $\eta_i=2$. The gyrofluid model is compared to linear kinetic theory. The ideal MHD result is shown for comparison and to emphasize the kinetic destabilization of the KBM below the ideal β_c at finite η_i.

transport below the calculated ideal stability limit, and its accurate description is important for a complete transport model.

IV. NONLINEAR SIMULATION RESULTS

Nonlinear simulations are carried out in a toroidal flux tube geometry[3] using an updated, massively parallel version of the GRYFFIN gyrofluid code. As many prior core transport studies have been undertaken in the zero β limit, it is of great interest to explore the functional dependence of transport on β. To this end, a series of six simulations is carried out with fixed profiles ($R/L_n=3$, $q=2$, $s=1$, $\eta_i=\eta_e=3$, $\tau=1$) but varying β from zero to 1%, approaching the ideal ballooning limit ($\beta_c=1.1\%$). A simple $s-\alpha$ shifted circle equilibrium is used in this study, with the Shafranov shift parameter (α) chosen to be consistent with β, though the code is capable of general equilibrium geometry. At moderate β, the ITG is the linearly dominant mode, though its growth rate decreases steadily with β. The KBM is dominant only in the $\beta=1\%$ case, though it is unstable at lower β. All simulations employ a 128×96 Fourier space grid in the radial and poloidal directions and 32 real space grid points along the field. Ap-

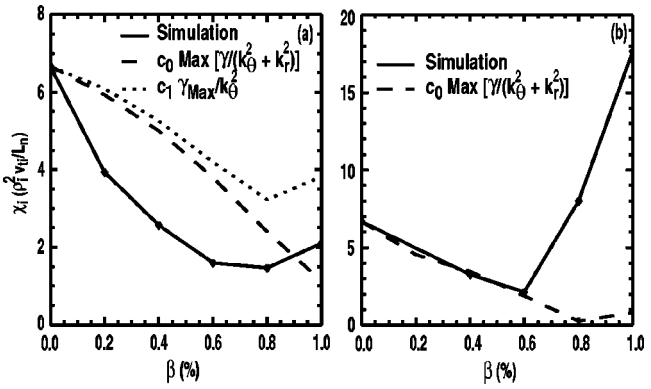

FIG. 3. Ion heat conductivity (χ_i) predicted by nonlinear gyrofluid simulations vs β, (a) without and (b) with electron dissipation. Note the different y-axis scales in the two plots. Simple mixing length estimates fitted to the $\beta=0$ result are shown for comparison.

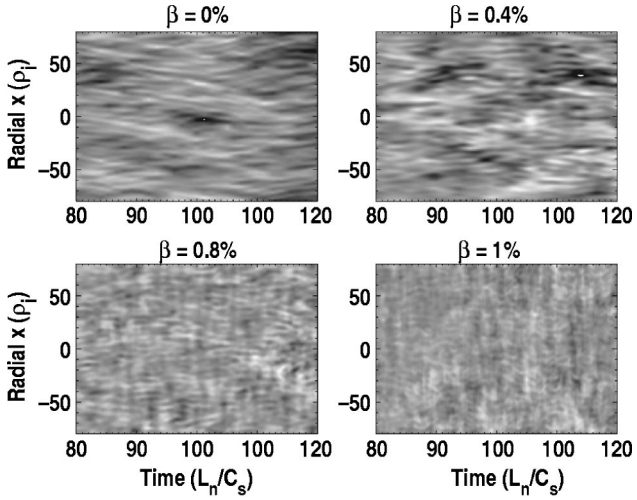

FIG. 4. Contour plots of the electrostatic potential on the outer midplane vs time and radius, at four values of the plasma β (0%, 0.4%, 0.8%, 1%). A qualitative change in turbulence timescales occurs as β approaches the ideal ballooning limit ($\beta_c=1.1\%$).

proximately 10^5 time steps of $5\pm2\times10^{-2}\,L_n/v_A$ have been evolved in each finite β case. Heat transport is found to be dominated by $\mathbf{E}\times\mathbf{B}$ fluctuations in all cases, with the magnetic flutter term smaller by at least an order of magnitude.

The variation of the time averaged steady-state ion heat conductivity (χ_i) with β, from simulations without electron Landau damping or collisions, is shown in Fig. 3(a). Two simple mixing length estimates, with constants fit to the $\beta=0$ simulation results, are also shown. Here the nonlinear behavior of the system can be qualitatively understood in terms of linear physics. For $\beta/\beta_c\lesssim1/2$, the conductivity decreases with β due to the finite β stabilization of the ITG mode. As β approaches β_c, the KBM is becoming unstable and appears to be driving an increase in χ_i (despite the fact that the ITG mode still has the higher growth rate).

The addition of electron Landau damping (using the electron/deuterium mass ratio) breaks the isothermal electron constraint, and changes the nonlinear behavior of the system dramatically. [A small amount of collisions, ($\hat{\nu}_{ei}=5\times10^{-5}$), was also included in these runs but has little effect.] The linear growth rate spectrum, and hence simple mixing length estimates of χ_i, change only modestly. For $\beta/\beta_c\lesssim0.5\%$, the simulation χ_i is similar to that in the dissipationless case. However, the introduction of electron dissipation through Landau damping increases the steady state χ_i by a factor of five at $\beta=0.8\%$ and by a factor of 8 at $\beta=1.0\%$, as illustrated in Fig. 3(b). In finite-β simulations with electron Landau damping, significant particle and electron heat transport are also measured. The diffusivity and electron heat conductivity scale similarly to χ_i but are reduced in magnitude by a factor of 3–4 in this case.

Figure 3 allows a comparison between earlier electrostatic predictions of transport (the $\beta=0$ point on the plot), and the electromagnetic prediction (using the physical β value). Normalization factors are unchanged in this comparison, hence the impact of finite β is to decrease predicted heat transport at small values of β/β_c, and to increase it as β/β_c approaches unity. It is important to note that the ratio β/β_c (roughly proportional to the MHD α factor), rather than β itself, should be used to gauge the importance of these finite β effects. In tokamaks, finite β effects tend to be larger toward the edge, where sharp gradients and large q values push the plasma close to the local ideal ballooning limit (β_c) despite the small absolute value of β. In the inner core region, pressure profiles tend to be flatter and q smaller, leading to relatively small values of β/β_c, despite the relatively large β values in the core.

The increase in χ_i as the ideal ballooning limit (β_c) is approached corresponds to a qualitative change in the turbulent dynamics, illustrated by Fig. 4. The eddy turnover time for the $\beta=1\%$ case is roughly a factor of 4 shorter than for the low $\beta/\beta_c=0\%-0.4\%$ cases, a change comparable to the linear difference in frequency between between the ITG and KBM at these parameters. Short-lived, radially extended streamers appear in the $\beta=1\%$ case, similar to those observed in collisional simulations.[24]

The transition from predominantly electrostatic ion-drift wave turbulence to Alfvénic turbulence can be quantified by the ratio of the mean square parallel electric field ($E_\parallel=-\nabla_\parallel\phi-\partial A_\parallel/\partial t$) to its electrostatic constituent, $\nabla_\parallel\phi$, shown in Fig. 5. In the usual (electrostatic) model of ion drift wave turbulence, this ratio is taken to be one, and magnetic fluctuations are neglected. In contrast, in ''ideal'' Alfvénic turbulence, magnetic induction exactly balances $\nabla_\parallel\phi$ and the ratio is zero. Figure 5 demonstrates that the electrostatic approximation can break down at modest values of $\beta/\beta_c\sim1/2$, and that the turbulence becomes predominantly Alfvénic as the ideal ballooning limit is approached. This transition is hindered somewhat by the presence of electron dissipation, which allows force balance to be achieved at large $E_\parallel$, even when $\nabla_\parallel n_e$ is small.

Steady state density and temperature fluctuation spectra have been extracted from the simulations and show a number of similarities to fluctuation measurements.[39,40] The radial spectra peak at zero, while the poloidal spectra peak at poloidal wave number $k_\theta=0.20\pm0.05\,\rho_s^{-1}$, nearly independent of β. The width of the peaks decreases significantly with β, with the full width at half maximum dropping

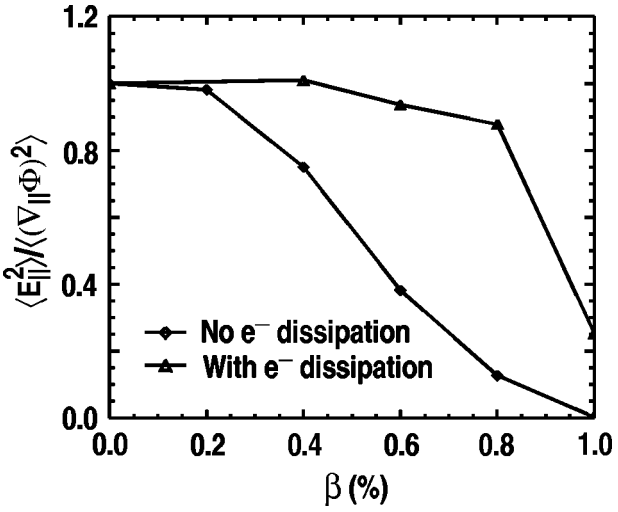

FIG. 5. The mean squared parallel electric field divided by its electrostatic component illustrates the transition from electrostatic to Alfvénic turbulence as β is increased.

roughly a factor of 3 as β increases from 0% to 1%. The simulations produce ion temperature spectra nearly identical in shape to the density fluctuation spectra, with a ratio of the relative temperature fluctuations to the relative density fluctuations of 2 ± 0.5, largely independent of parameters, similar to the measured behavior of carbon fluctuations.[40] Further investigation using the detailed geometry and parameters from the experiment is needed to confirm this agreement.

An important limitation of electrostatic simulations has been their inability to predict the dramatic increase in heat conductivity often seen in the outer $\sim$30% of tokamak plasmas. The increase in χ_i at higher $\alpha=-Rq^2\beta'\sim\beta/\beta_c$ seen in electromagnetic simulations is a candidate to explain the observed behavior, because while β itself decreases in the outer regions of tokamak plasmas, α often increases due to sharp gradients and increasing q. A preliminary study using parameters from a Tokamak Fusion Test Reactor[41] low confinement mode shot has indeed found that electromagnetic simulations predict much larger fluxes than electrostatic simulations of the outer region, bringing the simulation results into better agreement with measured fluxes.[28] Note however that effects such as certain nonlinear instability mechanisms (Refs. 25 and 24 and references therein) and electron gyroradius scale instabilities (e.g., ETG) may also be important in the outer edge region.

V. DISCUSSION

In summary, a model has been developed for the efficient simulation of long mean-free-path plasma turbulence including magnetic fluctuations and nonadiabatic passing electron dynamics. The model has been implemented in nonlinear three-dimensional toroidal flux-tube simulations, which exhibit fluctuation spectra with several characteristics in common with measurements. A transition from nearly electrostatic ion-drift turbulence to Alfvénic turbulence is observed to occur as β is increased above a threshold value of roughly half the ideal ballooning limit (β_c). The scaling of heat transport with β/β_c has been explored, and ion heat conductivity is found to decrease with β far from the ideal ballooning limit, but to increase with β as the ballooning limit is approached. In the presence of electron Landau damping, this increase in heat transport with beta can be dramatic and can occur significantly below the ideal ballooning threshold, perhaps helping to explain the high heat conductivity measured in the outer region of many tokamak experiments. Interesting future work could include comparing these nonlinear results with recently developed fully kinetic electromagnetic codes, and more detailed comparisons with experiments.

ACKNOWLEDGMENTS

This work was supported by United States Department of Energy Contract Nos. DE-FG03-95ER54309 and DE-AC02-76CH03073, and by a National Science Foundation fellowship. The authors wish to thank M. A. Beer and W. Dorland for many useful discussions, for providing the massively parallel, electrostatic toroidal gyrofluid code that was the starting point of our calculations, and for help with the GS2 code. They also thank M. Kotschenreuther for helpful discussions and for the use of his gyrokinetic GS2 code. Computer resources were provided by the National Energy Research Supercomputer Center, and by the Los Alamos Advanced Computing Lab, as part of the computational grand challenge Numerical Tokamak Turbulence Project.

[1] A. M. Dimits, G. Bateman, M. A. Beer *et al.*, Phys. Plasmas **7**, 969 (2000).
[2] S. E. Parker, W. W. Lee, and R. A. Santoro, Phys. Rev. Lett. **71**, 2042 (1993).
[3] M. A. Beer and G. W. Hammett, Phys. Plasmas **3**, 4046 (1996); G. W. Hammett, M. A. Beer, W. Dorland, S. C. Cowley, and S. A. Smith, Plasma Phys. Controlled Fusion **35**, 973 (1993).
[4] R. E. Waltz, G. D. Kerbel, and J. Milovich, Phys. Plasmas **1**, 2229 (1994); R. E. Waltz, G. D. Kerbel, J. Milovich, and G. W. Hammett, *ibid.* **2**, 2408 (1995).
[5] A. M. Dimits, T. J. Williams, J. A. Byers, and B. I. Cohen, Phys. Rev. Lett. **77**, 71 (1996).
[6] Z. Lin, T. S. Hahm, W. W. Lee *et al.*, Science **281**, 1835 (1998).
[7] F. Jenko and B. D. Scott, Phys. Plasmas **6**, 2705 (1999); F. Jenko, W. Dorland, M. Kotschenreuther, and B. N. Rogers, *ibid.* **7**, 1904 (2000).
[8] T. M. Antonsen and B. Lane, Phys. Fluids **23**, 1205 (1980).
[9] E. A. Frieman and L. Chen, Phys. Fluids **25**, 502 (1982).
[10] W. W. Lee, Phys. Fluids **26**, 556 (1983).
[11] T. S. Hahm, W. W. Lee, and A. Brizard, Phys. Fluids **31**, 1940 (1988).
[12] G. Hammett and F. Perkins, Phys. Rev. Lett. **64**, 3019 (1990).
[13] W. M. Tang, Nucl. Fusion **18**, 1089 (1978).
[14] J. Dong, P. Guzdar, and Y. Lee, Phys. Fluids **30**, 2694 (1987).
[15] J. V. W. Reynders, Phys. Plasmas **1**, 1953 (1994).
[16] J. Q. Dong, W. Horton, and J. Y. Kim, Phys. Fluids B **4**, 1867 (1992).
[17] J. Y. Kim, W. Horton, and J. Q. Dong, Phys. Fluids B **5**, 4030 (1993).
[18] W. M. Tang, J. W. Connor, and R. J. Hastie, Nucl. Fusion **20**, 1439 (1980).
[19] C. Z. Cheng, Phys. Fluids B **25**, 1020 (1982).
[20] T. S. Hahm and L. Chen, Phys. Fluids **28**, 3061 (1985).
[21] M. Kotschenreuther, Phys. Fluids **29**, 2898 (1986).
[22] B.-G. Hong, W. Horton, and D.-I. Choi, Phys. Fluids B **1**, 1589 (1989).
[23] F. Zonca, L. Chen, and R. Santoro, Plasma Phys. Controlled Fusion **38**, 2011 (1996).
[24] B. N. Rogers and J. F. Drake, Phys. Rev. Lett. **79**, 229 (1997).
[25] B. Scott, Phys. Plasmas **7**, 1845 (2000).
[26] X. Xu and R. Cohen, Contrib. Plasma Phys. **38**, 158 (1998).
[27] A. Zeiler, J. F. Drake, and B. N. Rogers, Phys. Rev. Lett. **84**, 99 (2000).
[28] P. B. Snyder, ''Gyrofluid theory and simulation of electromagnetic turbu-

lence and transport in tokamak plasmas,'' Ph.D. thesis, Princeton University, 1999.
[29]P. B. Snyder and G. W. Hammett, ''A Landau fluid model for electromagnetic plasma microturbulence,'' Phys. Plasmas (submitted).
[30]P. B. Snyder, G. W. Hammett, and W. Dorland, Phys. Plasmas **4**, 3974 (1997).
[31]B. B. Kadomtsev and O. P. Pogutse, in *Plasma Physics and Controlled Nuclear Fusion Research 1984* (International Atomic Energy Agency, Vienna, 1985), Vol. 2, p. 69.
[32]Y. Chen and S. Parker, Phys. Plasmas **8**, 441 (2001).
[33]A. Brizard, Phys. Fluids B **4**, 1213 (1992).
[34]Z. Chang and J. D. Callen, Phys. Fluids B **4**, 1167 (1992); **4**, 1182 (1992).
[35]W. Dorland and G. W. Hammett, Phys. Fluids B **5**, 812 (1993).
[36]W. M. Tang, J. W. Connor, and R. J. Hastie, Nucl. Fusion **20**, 1439 (1980).
[37]M. Kotschenreuther, G. Rewoldt, and W. M. Tang, Comput. Phys. Commun. **88**, 128 (1995).
[38]F. Zonca, L. Chen, J. Q. Dong, and R. A. Santoro, Phys. Plasmas **6**, 1917 (1999).
[39]R. J. Fonck, G. Cosby, R. D. Durst *et al.*, Phys. Rev. Lett. **70**, 3736 (1993).
[40]H. T. Evensen, R. J. Fonck, S. F. Paul *et al.*, Nucl. Fusion **38**, 237 (1998).
[41]R. J. Hawryluk, S. Batha, W. Blanchard *et al.*, Phys. Plasmas **5**, 1577 (1998).